Available online at www.sciencedirect.com

ScienceDirect

Procedia Structural Integrity 33 (2021) 265–278

Structural Integrity Procedia

www.elsevier.com/locate/procedia

IGF26 - 26th International Conference on Fracture and Structural Integrity

Examining the effect of indentation separation on the properties of proteinaceous adhesive films made bone gelatine

Ashley Amanda Freeman*, Di Wan, Chiara Bertolin

Department of Mechanical and Industrial Engineering, Norwegian University of Science and Technology, Richard Birkelands vei 2b, 7491 Trondheim, Norway

Abstract

Understanding the mechanical behaviour and properties of artists' materials is helpful for evaluating the failure of their structures during exhibition in confined spaces. Generally, macro-sized mock-ups of artists' materials are conventionally used to approximate the mechanical properties of historic materials. Although with newly adopted small-scale engineering methods, such as indentation, mechanical features can now be directly exploited from micro-sized samples taken from artworks.

When preparing for indentation tests a set of empirical rules are often followed, increasing the validity of the obtained results. These rules stress the importance of sample preparation and parameter selection. For sub-millimetre sized samples selecting appropriate spaced indents, that maximize the testing area while avoiding interference for sharp tip indenters, is essential.

This work focuses on the process of selecting optimal indent separation for proteinaceous adhesives derived from bones of bovine bone. Here a range of distances with two different originations are evaluated on mock-ups, allowing for the authors to examine the relationship between indent spacing and the obtained material properties. This first step of testing mock-ups is essential, as it assists in developing a comprehensive measuring procedure which takes into consideration the dimensional and geometrical restrictions of historic materials.

Keywords: Minimum spacing; Proteinaceous adhesives; Mechanical properties; Nanoindentation; Multivariate analysis

* Corresponding author
E-mail address: ashley.a.freeman@ntnu.no

10.1016/j.prostr.2021.10.033

1. Introduction

The use of proteinaceous adhesives (animal glues) is often dated back to ancient Egypt, although the exact emergence is unknown. Nevertheless, the first commercial manufacture of glue was founded in the late 17th century, with the first patent being registered half a century later, in 1754 (Bogue, 1922). This patent focused on a specific type of glue prepared from fish (fish glue) (Bogue, 1922), however, animal glues can be produced from various mammalian and fish species. Generally, animal glues are derived from the collagen of mammalian or fish through hydrolysis. Though, the triple helix nature of collagen dictates its dissolution, as such different pre-treatments (acidic or alkaline), as well as elevated temperatures, are often used to cleave the intra/intermolecular polypeptide bonds. Aiding in the extraction process. Depending on the collagen source, production process, and method of preparation (e.g., concentration or additives), animal glues will display different chemical, physical, and mechanical behaviours (Schellmann, 2007).

Gelatine is extremely versatile and has been examined as a material for various pharmaceutical, biomedical, and food industry applications. Furthermore, adhesives based on gelatine (i.e., animal glues) are multipurpose materials and can be used as binding medium of paints (e.g., distemper paint), as a barrier layer (e.g., size which is a layer of adhesive applied to a wooden panel to seal it), as a consolidant (e.g., re-adhering delaminated painted surface), or as an adhesive to bond wooden joints. Commercially accessible glues are typically produced from hide (bovine or small mammal), bone (bovine or porcine), and fish (bone, scales, or swim bladder).

Conventionally, mechanical properties of artists' materials are characterised by means of macroscopic tensile tests of laboratory prepared films. Although, more recently, cultural heritage material scientists have more readily adopted the use of nanoindentation experiments to characterize sub-millimetre sized samples taken from artworks. Indentation has been successfully adapted for the characterization of historic samples taken from 17th (Tiennot et al., 2020) and 19th (Salvant et al., 2011) century oil paintings, as well as embedded (Fujisawa & Łukomski, 2019) and nonembedded laboratory prepared films (Sturdy et al., 2020; Wright et al., 2014). Nanoindentation has the capacity to produce quantitative results from historic samples, but like other small volume samples, consideration must be given to many factors including spacing between indentation tests.

Determining minimum spacing for indentation has been approached in several different ways. Although the most followed criterium was proposed by Samuels and Mulhearn (1957). They suggested a distance of at least three times the lateral dimension of the indent, which is about 20 times the indentation depth for a Berkovich tip. Since then, a few research groups have applied and evaluated the criteria for optimizing indent spacing of various materials. Zhao and Ovaert (2010) studied the relationship between indent spacing and elastic modulus of titanium and steel alloys. Reliable results were obtained when a spacing greater than 10 times the indentation depth for a Berkovich was used. Sudharshan Phani and Oliver (2019) examined the effect of spacing on various materials and found that for a Berkovich indenter a minimum spacing of 10 times the indentation depth can result in accurately obtained hardness values. The authors went on to say that the obtained hardness values were more greatly influenced by spacing than by the number of neighbouring indents within an array. Jiang et al. (2020) examined the effect of spacing on the mechanical properties of polystyrene. Their results suggest that a distance of at least 10 times the maximum indentation depth should be used for indents performed in a single row/column, whereas a spacing of at least 15 times the maximum indentation depth should be used within an array. Lastly, the ISO standard for indentation of metallic materials (ISO, 2015) can be consulted when determining minimum spacing. For materials other than ceramics or metals, it suggests a minimum distance of at least 10 times the indentation diameter. However, shorter distances can be used if experimental data obtained at these closer distances are comparable to those obtained at the recommended separation.

In the current research, the mechanical behaviour of a single proteinaceous adhesive is evaluated using quasi-static indentation tests. Here a range of distances with two different originations are evaluated on mock-ups, allowing for the authors to examine the relationship between indent spacing and the obtained material properties. This first step of testing mock-ups is essential, as it assists in developing a comprehensive measuring procedure which takes into consideration the dimensional and geometrical restrictions of historic materials.

Nomenclature

h	Displacement, penetration depth
Q1	First quartile
BONE	Glue made from the animal bones
H	Hardness
d	Indentation separation
ISO	International Organization for Standardization
IQR	Interquartile range
P	Load
P-h	Load-displacement
h_{max}	Maximum displacement
P_{max}	Maximum load
O-P	Oliver and Pharr
E_r	Reduced modulus
SE	Standard error
Q3	Third quartile

2. Materials and methods

2.1. Test specimen

4 % w/w (glue granules/water) proteinaceous adhesive films were produced by solubilising glue material in distilled water for 24 hours. After which, the solutions were heated in a double boiler and mixed until the suggested heating temperature was reached (60-65 °C). Once the solutions reached room temperature (~22 °C), 20 ml aliquots were added to Petri dishes and allowed to dry in ambient conditions for at least seven months. The process of making the adhesive films is shown in Fig. 1. See Table 1 for additional product information.

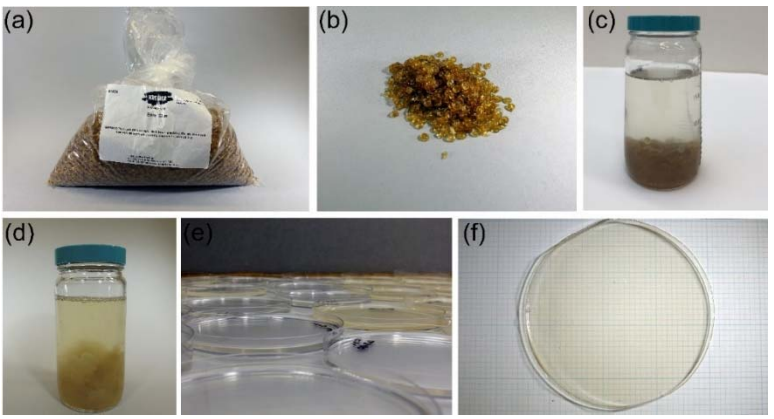

Fig. 1. Illustration of adhesive film making process; (a) commercial product, (b) closeup of granular gelatine before soaking in water, (c) granular gelatine after addition of water, (d) granular gelatine after addition of 24 immersion in water, (e) casting films, and (f) adhesive film after drying in ambient conditions.

Table 1. Product information from manufacture

	63000 Bone Glue	Reference
Form	Pearls; grains	(Kremer-Pigmente, 2020)
Animal part	Cow bone	(Kremer-Pigmente)
Country of Origin	China	
Bloomgrams	120 +/- 20	
Millipascal Seconds	36 – 44	
Chemical characterisation	Bone glue	(Kremer-Pigmente, 2016)
pH	5.75 – 7.0	
Solubility in water	soluble	

2.2. Experimental procedure

Specimens were cut from the adhesive films using a scalpel, resulting in nominal length and width of 1 cm. These specimens were then fixed to a metal stage using Tipp ex® correction fluid. A thin layer of the fluid was applied to the metal stage, and when drying the specimens were firmly placed.

Experiments were performed using a Hysitron TI 950 TriboIndenter (Bruker, USA) equipped with a Berkovich probe. To examine the effect of spacing, two different orientations were carried out with sequential indents (Fig. 2).

- Three sequential indents in a row or a column were performed in the x and y directions with varying separation per row/column (3, 6, 9, 14, 35, 100 µm). Herein, the x and y directions refer to random directions forming a cartesian coordinate system (thus they can be used to describe the 2D surface of the specimen) and they do not refer to any physical orientation regarding the sample production and preparation, etc.

- Then, an indentation array of 3 × 3 was carried out using an indentation separation (d) of 6, 9, 14, 35, and 100 µm.

In both cases, the load function consisted of a 1 second linear loading to the maximum load of 10000 µN, followed by a 0.5 second dwell at maximum load, and a 1 second linear unloading. Each testing orientation was performed at least three times.

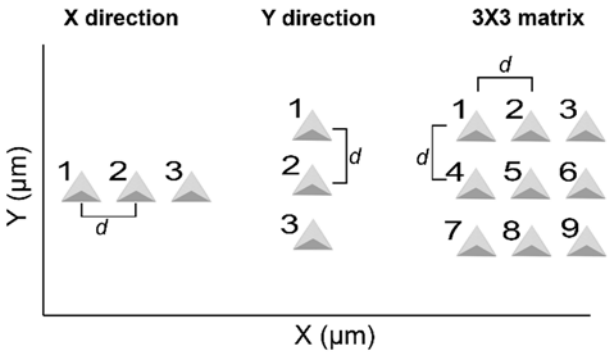

Fig. 2 (a) schematic showing separation in the x and y directions, and the 3× 3 indentation array, where *d* denotes separation.

A typical load-displacement curve recorded by the indentation system is shown in Fig. 3. These curves were processed using Indentation software and the Oliver and Pharr method (Oliver & Pharr, 1992, 2004), which allowed for hardness (H) and reduced modulus (E_r) to be determined.

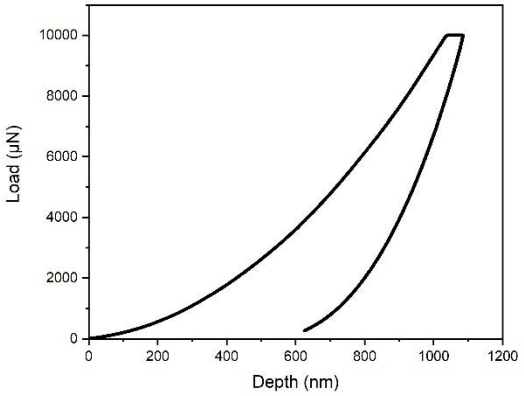

Fig. 3 Schematic of a typical load-displacement (*P- h*) curve obtained during this study.

2.3. Regression analysis

Regression analyses are common statistical modelling techniques that are applied to predict an output parameter from a set of input parameter(s). Whereas single regression models consist of an outcome data (dependent variable) and a predictor data (independent variable), multivariate regression models are applied in more complex relationships in which there are multiple independent variables. A multivariate regression equation would typically have the form of

$$y = b_0 + b_1 x_1 + b_2 x_2 \cdots b_n x_n \tag{1}$$

Expressing the relationship between the dependent (i.e., Ys) and independent (i.e., Xs) data.

Additionally, Eq.1 can be expressed as a matrix as presented as:

$$\begin{bmatrix} y_1 \\ \vdots \\ y_n \end{bmatrix} = \begin{bmatrix} 1 & x_1 \\ \vdots & \vdots \\ 1 & x_n \end{bmatrix} \begin{bmatrix} b_1 \pm SE_{b_1} \\ \vdots \vdots \vdots \\ b_n \pm SE_{b_n} \end{bmatrix} \tag{2}$$

where, *SE* denotes the standard error. Additionally, Eq. 2 can be simply as:

$$Y = (b \pm SE)X \tag{3}$$

where X is a matrix consisting of the independent data, b is comprised of the regression vector, whose values or parameters are estimated by the analysis procedure, and Y is the response data vector.

3. Results and Discussion

This study aimed to evaluate the influence of indentation spacing on the obtained mechanical properties of a gelatine-based adhesive film. In particular, box plots were used to examine the relationships between spacing and the film's mechanical properties, and regression analysis was performed, allowing investigation into the effects of testing location on the obtained results.

Fig. 4 shows the maximum displacement, indentation hardness, and reduced modulus are presented as box and whiskers plots. It is worthy to note that different independent data (Xs) have different scales and therefore have a different median, standard deviation, and range. Parameters describing the distribution of the obtained results and are described by the median, mean, first quartile (Q1; the 25th percentile), third quartile (Q3; the 75th percentile), the interquartile range (IQR which is the difference between Q3 and Q1), and outliers (data that lies 1.5 x IQR below or above Q1 or Q3, receptivity) as shown in the illustration in Fig. 4. Here indentations tests, regardless of the testing orientation (x-direction, y-direction, and 3×3 matrix) were analysed with the spacing between the indents as the grouping factor. Thus, resulting in six groups (3, 6, 9, 14, 35, 100 µm). The indent spacings are arranged left to right, from least to greatest spacing. The results represent 24–60 measurements per spacing group. Additionally, the numerical data of each box plot has been tabulated and placed into Appendix A.

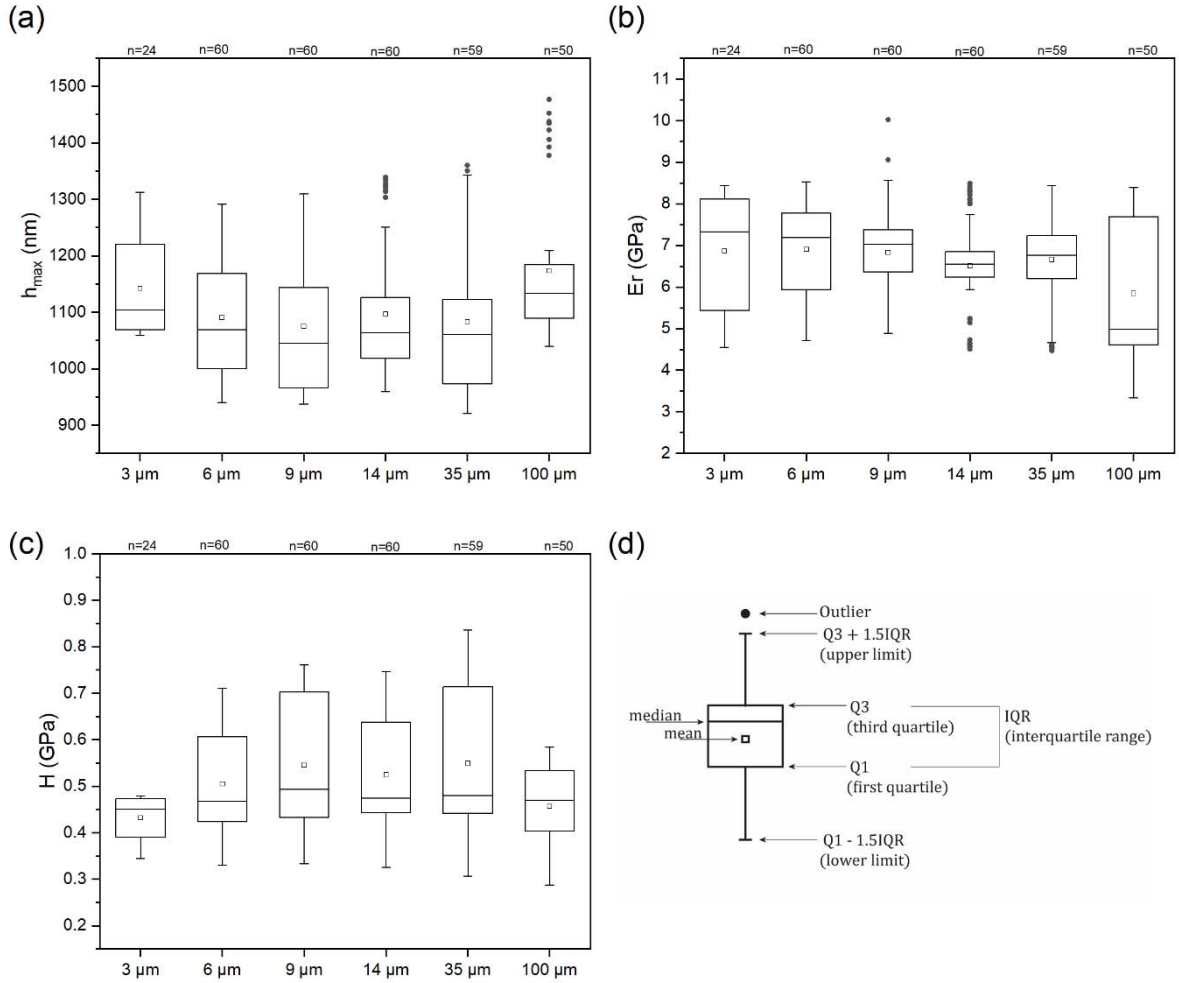

Fig. 4 Box and whisker plots of maximum indentation depth (a) reduced modulus (b), and hardness (c), where n on top of each plot is used to denote the number of data points. These boxes display the inter-quartile range (lower and upper quartiles), in which the upper and lower whiskers represent the maximum and minimum. As depicted in the didactic (d), the whiskers extend to 1.5 times the interquartile range. Additionally, the midline within the box represents the median and the small box is used to denote the mean value. Further, suspected outliers are indicated by circles shown as dots located above and below the whiskers.

It can be observed in Fig. 4 that outliers were identified in both the h_{max} and E_r data sets. In particular, outliers were detected in three cases for both $h_{\max}$ and E_r. The outliers within the h_{max} data set consisted of indents performed in all three orientations (x-direction, y-direction, and 3× 3 matrix). The two outliers that were found at a spacing of 9 μm were from sequential indents (indent two and three) carried out in the y-directions, while the 23 outliers detected at a spacing of 14 μm were from all three orientations (11 indents performed in the y direction, three sequential indents performed in the x-direction, and nine indents all from the same 3× 3 matrix). The seven outliers identified in the data set obtained at a spacing of 35 μm, all belong to the same 3×3 matrix.

Concerning the outliers identified from the E_r data, all belong to tests performed in the 3×3 matrix orientation, in which two outliers were detected at a spacing of 9 μm and nine outliers were identified for indents performed at spacings of 14 and 35 μm. Further, all of these outliers belonged to the first 3× 3 matrix performed at that specific spacing. Lastly, no outliers were identified for the hardness data sets.

Fig. 4b presents the distributions of reduced moduli at the different spacings, in which the box, or interquartile range, is an illustration of the middle 50% of the data. Additionally, the horizontal lines within these boxes represent the median values at each spacing, whereas the small squares indicate the mean values. Herein median values and IQR are used to describe the obtained data. In the case of E_r, the largest and smallest interquartile ranges were exhibited at a spacing of 100 μm (IQR=3.07 GPa) and 14 μm (IQR=0.62 GPa). Even Though in the latter spacing, the data displays a higher precision, there are numerous outliers. Further, the large IQR for spacing in 100 μm is suggestive of a higher variability in the data than those obtained at the other spacing. This situation is indicative of possible bias, most likely resulting from inhomogeneity of the material properties, as this distance is at least four times larger than the minimum $h_{\max}$ and thus indents do not overlap. Consequently, for the purpose of this study the obtained parameters at 35 μm are considered to have no significant influence from indent spacing and have a better precision, and are used as a reference to evaluate the more closely spaced indents (3-14 μm). Moreover, when comparing the E_r between 3 and 35 μm (excluding 100 μm), median values ranged between 7.33 and 6.56 GPa with a slight decreasing trend. It can be observed from the plot that the median values of the modulus begin to stabilize between a spacing of 9 and 14 μm, especially when comparing these results with those obtained at 35 μm (6.77 GPa; IQR 1.04 GPa). The median values of E_r obtained at a spacing of 9 and 14 μm are 7.02 and 6.56 GPa, respectively, with IQRs < 1.02 GPa. In comparison, a slight increase in the median value of hardness is observed as the distance between indents increases (Fig. 4c). For the hardness values between 3 and 35 μm, median values ranged between 0.45-0.49 GPa with IQR< 0.27 GPa. Further, at the spacing in which the parameters begin to stabilize, and greater (spacing of 9 - 35 μm), median values ranged between 0.47-0.49 GPa with an IQR between 0.20-0.27 GPa.

Herein, multivariate regression analysis was performed on the indentation data using Microsoft Excel. The regression equations were applied to describe how the obtained parameters ($h_{\max}, H, E_r$) depend on the location of testing (Cartesians coordinates of the indent). A simple regression equation was first applied. If this model did not represent the data, then more complex models were applied (e.g., 2nd degree polynomials). Like R^2 values, adjusted R^2 values indicate how well a predictive model fits the data set; however, unlike R^2, it adjusts for the number of variables within the model. And thus, adjusted R^2 is more ideal when comparing models with different numbers of variables. For the purpose of this study, the adjusted R^2 was used to examine the goodness-of-fit, and therefore the accuracy, for each predictive model. Subsequently, R^2 values were calculated to examine the correlation between the measured and the predicted parameters from the proposed models (Origin Pro 2018b, Originlab Co, MA, USA).

All data, regardless of the testing orientation, was examined using the indentation separation as the grouping factor. Tables 3 provides the statistical model summaries for the prediction of the three obtained parameters: $h_{\max}, H,$ and E_r. Additionally, in each model, the x and y location of the indents (i.e., descriptive variables) were denoted by x_1 and x_2, respectively. For the proposed models, slightly more than half of the fits consisted of five coefficients, while only two models consisted of two variables (100 μm spacing for $h_{\max}$ and H predictions). And in most cases, the P values of the coefficients were found to be higher than significance level of 5% (See Appendix B). Further, R^2 values of the

proposed models for $h_{\max}$, H, and E_r ranged from -0.04 to 0.82, -0.02 to 0.77, and 0.28 to 0.89, respectively (Fig. 5-7).

Table 3. Summary of regression models for $h_{\max}$, H, and E_r. Additionally, adjusted R^2 (Adj. R^2) values show the fit of the multivariate model. Additionally, the Cartesians coordinates of the indent location, x and y, are denoted by x_1 and x_2, respectively.

Spacing (μm)	Number of variables	Model	Adj. R^2
Regression models for maximum displacement, $h_{\max}$			
3	5	$y_{3h_{max}} = \left(-1.66\times10^{6} \pm 8.74\times10^{5}\right) + \left(-1.78\times10^{4} \pm 9.23\times10^{3}\right)x_1 + \left(1.73\times10^{2} \pm 5.00\times10^{3}\right)x_2 + \left(-8.91 \pm 2.85\times10^{1}\right)x_1x_2 + (-4.75\times10^{1} \pm 2.44\times10^{1})x_1^2 + (\pm 1.68\times10^{1})x_2^2$	0.82
6	3	$y_{6h_{max}} = \left(-5.40\times10^{4} \pm 2.74\times10^{4}\right) + \left(-2.91\times10^{2} \pm 1.45\times10^{2}\right)x_1 + {}^{3}\left(-4.57\times10 \pm 2.06\times10^{3}\right)x_2 + (-2.41\times10^{1} \pm 1.09\times10^{1})x_1x_2$	0.11
9	3	$y_{9h_{max}} = \left(-4.84\times10^{4} \pm 3.12\times10^{4}\right) + \left(-2.62\times10^{2} \pm 1.65\times10^{2}\right)x_1 + \left(-4.11\times10^{3} \pm 2.37\times10^{3}\right)x_2 + (-2.17\times10^{1} \pm 1.25\times10^{1})x_1x_2$	0.06
14	5	$y_{14h_{max}} = \left(-1.14\times10^{6} \pm 2.32\times10^{6}\right) + \left(-1.23\times10^{4} \pm 2.50\times10^{4}\right)x_1 + \left(8.11\times10^{2} \pm 6.30\times10^{3}\right)x_2 + \left(4.78 \pm 3.40\times10^{1}\right)x_1x_2 + \left(-3.32\times10^{1} \pm 6.71\times10^{1}\right)x_1^2 + (-1.29 \pm 2.10)x_2^2$	-0.04
35	5	$y_{35h_{max}} = \left(9.02\times10^{-5} \pm 1..35\times10^{2}\right) + \left(-2.77\times10^{1} \pm 2.15\times10^{2}\right)x_1 + \left(3.87 \pm 3.27\times10^{3}\right)x_2 + \left(3.59\times10^{-1} \pm 1.76\times10^{1}\right)x_1x_2 + \left(-1.34\times10^{-1} \pm 1.15\right)x_1^2 + (-9.49\times10^{-1} \pm 1.37)x_2^2$	0.03
100	2	$y_{100h_{max}} = -1.531\times10^{-1}(\pm 1.07\times10^{2}) - 5.71\times(\pm 5.95\times10^{-1})x_1 - 3.27(\pm 7.28\times10^{-1})x_2$	0.28
Regression models for reduced modulus, E_r			
3	5	$y_{3H} = (6.96\times10^{2} \pm 5.06\times10^{2}) + (7.43 \pm 5.34)x_1 + (2.59\times10^{-1} \pm 2.89)x_2 + (6.66\times10^{-3} \pm 1.50\times10^{-2})x_1x_2 + (1.97\times10^{-2} \pm 1.41\times10^{-2})x_1^2 + (-4.56\times10^{-2} \pm 9.72\times10^{-3})x_2^2$	0.77
6	3	$y_{6H} = (2.55\times10^{1} \pm 2.83\times10^{1}) + (1.33\times10^{-1} \pm 1.50\times10^{-1})x_1 + (2.11 \pm 2.12)x_2 + (1.12\times10^{-2} \pm 1.12\times10^{-2})x_1x_2$	0.18
9	3	$y_{9H} = (2.66\times10^{1} \pm 3.32\times10^{1}) + (1.39\times10^{-1} \pm 1.76\times10^{-1})x_1 + (2.19 \pm 2.53)x_2 + (1.16\times10^{-2} \pm 1.34\times10^{-2})x_1x_2$	0.23
14	5	$y_{14H} = (4.66\times10^{2} \pm 2.38\times10^{3}) + (5.08 \pm 2.56\times10^{1})x_1 + (-1.17 \pm 6.46)x_2 + (-6.49\times10^{-3} \pm 3.49\times10^{-2})x_1x_2 + (1.38\times10^{-2} \pm 6.88\times10^{-2})x_1^2 + (9.10\times10^{-4} \pm 2.16\times10^{-3})x_2^2$	0.22
35	5	$y_{35H} = (-7.01\times10^{-7} \pm 1.48\times10^{-1}) + (-2.93\times10^{-2} \pm 2.36\times10^{-1})x_1 + (6.42\times10^{-1} \pm 3.59)x_2 + (3.28\times10^{-3} \pm 1.94\times10^{-2})x_1x_2 + (-1.35\times10^{-4} \pm 1.27\times10^{-3})x_1^2 + (3.46\times10^{-4} \pm 1.51\times10^{-3})x_2^2$	0.23
100	2	$y_{100H} = (4.41\times10^{-4} \pm 8.85\times10^{-2}) + (-2.43\times10^{-3} \pm 4.92\times10^{-4})x_1 + (-1.42\times10^{-4} \pm 6.02\times10^{-4})x_2$	-0.02
Regression models for hardness values, H			
3	5	$y_{3Er} = \left(1.57\times10^{43} \pm 1.09\times10^{4}\right) + \left(1.68\times10^{2} \pm 1.15\times10^{2}\right)x_1 + \left(2.09 \pm 6.24\times10^{1}\right)x_2 + \left(1.45\times10^{-1} \pm 3.23\times10^{-1}\right)x_1x_2 + \left(4.45\times10^{-1} \pm 3.04\times10^{-1}\right)x_1^2 + (-1.17 \pm 2.10\times10^{-1})x_2^2$	0.89
6	3	$y_{6Er} = (1.15\times10^{3} \pm 2.28\times10^{2}) + \left(6.03 \pm 1.21\right)x_1 + (9.27\times10^{1} \pm 1.71\times10^{1})x_2 + (4.90\times10^{-1} \pm 9.05\times10^{-2})x_1x_2$	0.33
9	3	$y_{9Er} = (9.69\times10^{2} \pm 2.55\times10^{2}) + \left(5.09 \pm 1.35\right)x_1 + (8.13\times10^{1} \pm 1.94\times10^{1})x_2 + (4.30\times10^{-1} \pm 1.03\times10^{-1})x_1x_2$	0.28

14	5	$y_{14Er} = (1.24\times10^{4} \pm 1.64\times10^{4}) + \left(1.33\times10^{2} \pm 1.76\times10^{2}\right)x_1 + (-2.31 \pm 4.45\times10^{1})x_2 + \left(-2.09\times10^{-2} \pm 2.40\times10^{-1}\right)x_1x_2 + (3.58\times10^{-1} \pm 4.74\times10^{-1})x_1^2 + (2.31\times10^{-2} \pm 1.48\times10^{-2})x_2^2$	0.50
35	5	$y_{35Er} = \left(2.61\times10^{-5} \pm 8.98\times10^{-1}\right) + \left(2.25\times10^{-1} \pm 1.43\right)x_1 + \left(-6.61 \pm 2.18\times10^{1}\right)x_2 + \left(-4.26\times10^{-2} \pm 1.18\times10^{-1}\right)x_1x_2 + (1.78\times10^{-3} \pm 7.70\times10^{-3})x_1^2 + (2.14\times10^{-2} \pm 9.15\times10^{-3})x_2^2$	0.40
100	5	$y_{100Er} = \left(6.41\times10^{-5} \pm 6.51\times10^{-1}\right) + \left(-8.79\times10^{-1} \pm 5.30\times10^{-1}\right)x_1 + \left(8.50 \pm 6.99\right)x_2 + (4.13\times10^{-2} \pm 3.74\times10^{-2})x_1x_2 + (-4.29\times10^{-3} \pm 2.83\times10^{-3})x_1^2 + (1.14\times10^{-2} \pm 4.50\times10^{-3})x_2^2$	0.86

In all scenarios, regardless of the predicted parameter ($h_{\max}$, H, E_r), the proposed model for a spacing of 3 μm displayed an Adj. R^2 value of at least 0.77. Further, the predictive models used for this spacing contained five coefficients. These calculations suggest a dependency of the dependent variables on the independent variables (i.e., the predicted parameters are influenced by the location of testing). In detail, for the $h_{\max}$ spacing at 3 μm the multivariate model is accurate, and data are precisely indicating the possibility to predict the position of the next indent thus having maximum spatial influence; while at spacing where the outliers are present, the model's accuracy decreases together with the data precision revealing difficulty in simulating the position using the model. Although not at a spacing of 100 μm, it is also clear that it is easier to predict 3 × 3 matrix orientation with the multivariate model, while the x and y directions are those that report higher bias or deviation from the model (e.g., a higher total analytical error).

Moreover, as these indents exhibited a maximum displacement that ranged from 1058 to 1313 nm (Fig. 4a), it is unsurprising that the spacing of 3 μm is influencing the measured parameters. As mentioned previously, a spacing of at least 20 times the indentation depth is the most followed approach. Although more recently, various groups have shown that a less conservative approach can be taken; recent studies have suggested that a spacing of at least 10 times the maximum depth is sufficient for obtaining hardness and modulus values. Thus, if this less conservative approach were followed, then these depths would correspond to a separation of 11 to 13 μm. Additionally, the range in depth, could be suggestive of variation in material properties resulting from the previous indent or natural inhomogeneity within the material itself.

Whereas the predictive model of H at a spacing of 100 μm consisted of five coefficients, although with a slightly higher Adj. R^2 value (0.86) than those presented for a spacing of 3 μm, only two variables were used for predictive models of E_r and displacement. Similarly, the predictive models of $h_{\max}$ and E_r at 3 μm, the $h_{\max}$ and E_r models presented for at 100 μm suggest dependency of the dependent variables on the independent variables. At 3 and 100 μm the multivariate models are accurate, with a higher precision in the first case. Further, it is visible that the 3 × 3 matrix is more accurate, especially at high measured H, while this data set displays a larger bias in respect to the target value of the model at lower measured H. Although unlike the predictive models at 3 μm, this dependency is likely signifying the inhomogeneity of test specimen.

Lastly, it is of interest to examine the predictive models at which the median values of modulus and hardness begins to stabilize (i.e., 9 μm and 14 μm in Fig. 4b,c). For all predictive models presented for a spacing of 9 μm and 14 μm the models consisted of three and five variables, respectively. Further, the low Adj. R^2 values (<0.28) are suggestive of a lower dependence of the parameters on the testing location, than those from the predictive models of 100 μm and 3 μm, as discussed above.

To assess the relative quality of the predictive capabilities of these models, linear regressions were performed and the R^2 values indicative of the model accuracy are reported. Figs. 5- 7 present comparisons between measured and predicted parameters using the equations listed in Table 3. Here R^2 values are used to show goodness-of-fit, with high R^2 values being indicative of a good fit and low R^2 indicating an insufficient fit. Here the R^2 values range from 0.05 to 0.86, 0.41 to 0.92, and 4.80×10^{-4} for $h_{\max}$, E_r, and H, respectively. When comparing the models proposed during this study, those presented for a spacing of 3 μm consistently display the highest R^2 (>0.82). This could be resultant from the fact that all other models were developed using data from all three orientation; however, the majority of the data are from tests performed using 3× 3 matrix which is the easiest to model. Further, the models proposed for a spacing of 3 μm only consisted of tests performed in the x-direction and y-direction which displayed a higher bias.

Moreover, only the models presented for E_r, consistently give R^2 values which are greater than 0.32. This could suggest that for this data set, that multivariate analysis is more capable of investigating modulus values than displacement and hardness.

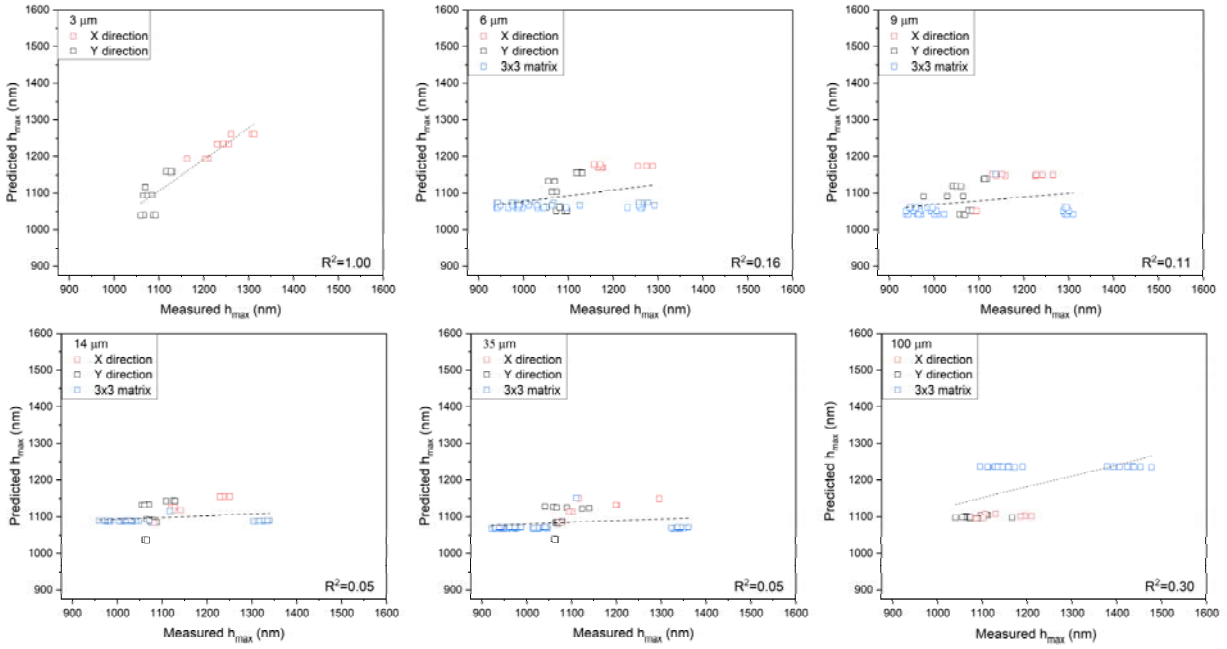

Fig. 5 Correlation between predicted and measured maximum displacement

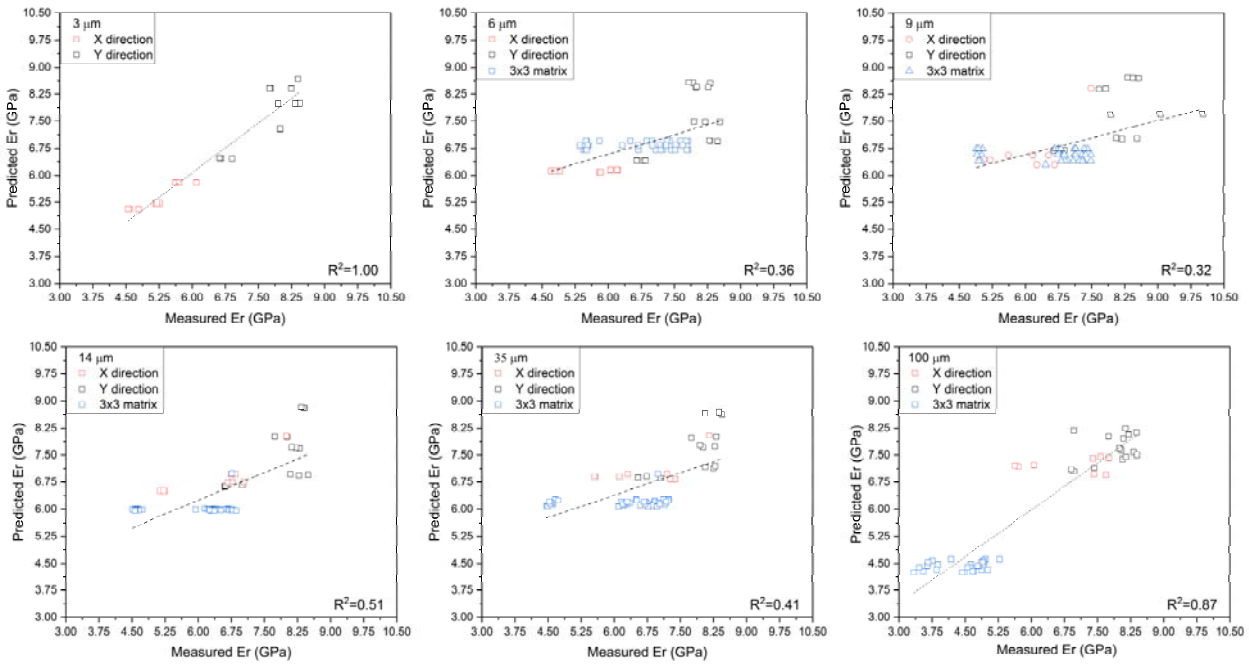

Fig. 6 Correlation between predicted and measured reduced modulus

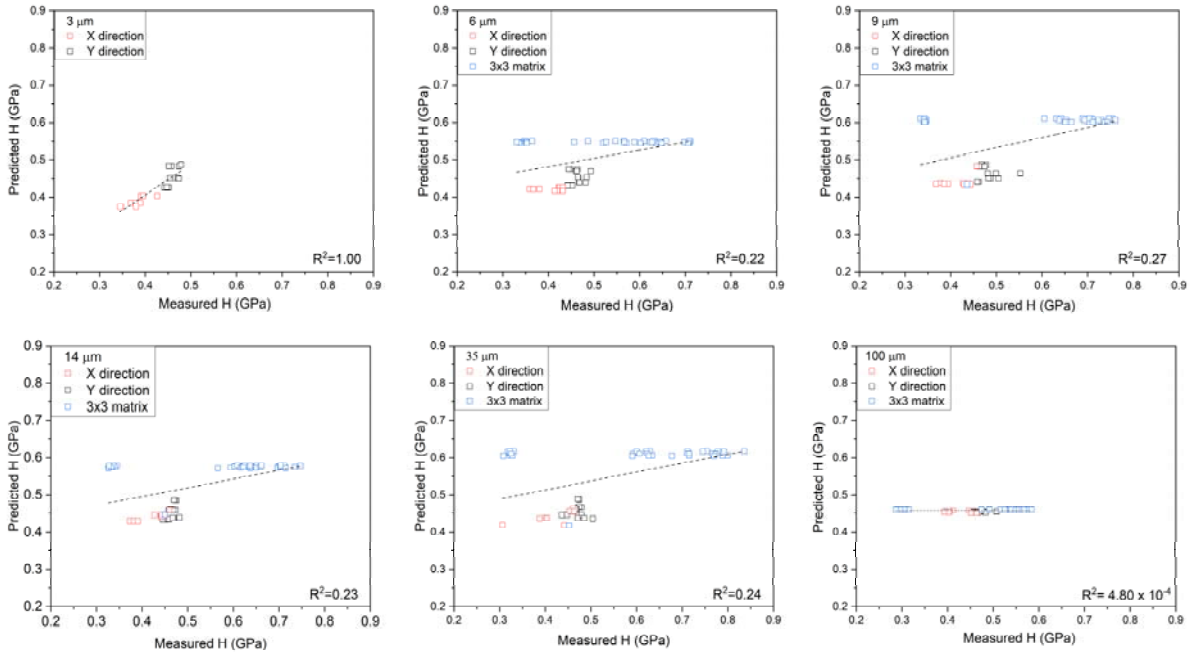

Fig. 7 Correlation between predicted and measured hardness

Conclusions

Investigating the spacing between indents is an essential part of developing a testing protocol for sub-millimetre sized samples. Conventionally, a spacing of 20 times the indentation depth was used until recently, when a few groups have shown that half this conservative spacing can be used for a range of materials. Within the limitations of this study, it was found that a spacing around 10 times the indentation depth can also be used to study adhesive films prepared from commercial bone gelatine. Complications were encountered when analysing the data obtained at 100 µm, which could be resulted from testing different responses of the material or from x- and y-directions which could be resulted in lower accuracy because of biases present. Further, it was found that this adhesive film displayed a median hardness and modulus ranging from 0.45-0.48 GPa and 6.77-7.33 GPa, respectively (when excluding data obtained at 100 µm). Additionally, median hardness and modulus at spacing between 9 and 35 µm (spacings which showed little to no effect on the obtained data) ranged from 0.47-0.49 GPa and 6.56 -7.02 GPa, respectively. Nonetheless, further work is required to determine the exact spacing at which this transition occurs. Finally, as only one material type was investigated (i.e., commercial bone glue), it would be of interest to determine whether similar results can be produced with different adhesive films.

Authors Contribution

A.A.F.: Writing—original draft preparation; Writing—review and editing; Visualization; Formal analysis.
D.W.: Investigation; Validation; Writing—review and editing.
C.B.: Formal multivariate data analysis and validation; Writing—review and editing; Supervision; Resources; Funding Acquisition.

Acknowledgements

This project was supported by the Sustainable Management of Heritage Buildings in a Long-term perspective (SyMBoL) Project (Project No. 274749).

Appendix A. Descriptive statistics for box plots of measured h_{max}, H, and E_r.

	N total	Mean	Standard Deviation	Minimum	1st Quartile (Q1)	Median	3rd Quartile (Q3)	Maximum	Interquartile Range (Q3 - Q1)
Maximum displacement, h_{max} (nm)									
3 µm	24	1142.21	86.71	1058.93	1069.27	1104.49	1220.15	1312.53	150.88
6 µm	60	1090.71	108.71	939.88	1000.30	1069.44	1168.68	1291.61	168.38
9 µm	60	1075.39	123.70	937.33	965.76	1045.31	1144.42	1309.46	178.66
14 µm	60	1097.37	114.32	959.33	1018.98	1064.01	1126.28	1250.50	107.30
35 µm	59	1083.41	133.02	921.16	973.34	1060.95	1123.07	1343.28	149.73
100 µm	50	1173.80	126.38	1039.64	1089.72	1133.86	1184.52	1209.14	94.79
Reduced modulus, E_r (GPa)									
3 µm	24	6.87	1.43	4.55	5.44	7.33	8.12	8.44	2.67
6 µm	60	6.91	1.04	4.71	5.94	7.18	7.78	8.53	1.84
9 µm	60	6.83	1.16	4.89	6.36	7.02	7.38	8.56	1.02
14 µm	60	6.51	1.13	5.94	6.23	6.56	6.85	7.74	0.62
35 µm	59	6.66	1.13	4.66	6.20	6.77	7.24	8.44	1.04
100 µm	50	5.85	1.70	3.34	4.62	4.99	7.69	8.40	3.07
Hardness values, H (GPa)									
3 µm	24	0.43	0.05	0.34	0.39	0.45	0.47	0.48	0.08
6 µm	60	0.51	0.12	0.33	0.42	0.47	0.61	0.71	0.18
9 µm	60	0.55	0.15	0.33	0.43	0.49	0.70	0.76	0.27
14 µm	60	0.52	0.13	0.33	0.44	0.47	0.64	0.75	0.20
35 µm	59	0.55	0.16	0.31	0.44	0.48	0.71	0.84	0.27
100 µm	50	0.46	0.09	0.29	0.40	0.47	0.53	0.58	0.13

Appendix B. Regression data

		P – values		
		H	E_r	h_{max}
3 µm	Intercept	0.19	0.17	0.07
	Variable 1	0.18	0.16	0.07
	Variable 2	0.93	0.97	0.97
	Variable 3	0.66	0.66	0.73
	Variable 4	0.18	0.16	0.07
	Variable 5	0.00	0.00	0.00
6 µm	Intercept	0.37	0.00	0.05
	Variable 1	0.38	0.00	0.05
	Variable 2	0.32	0.00	0.03
	Variable 3	0.32	0.00	0.03
9 µm	Intercept	0.43	0.00	0.13
	Variable 1	0.43	0.00	0.12
	Variable 2	0.39	0.00	0.09
	Variable 3	0.39	0.00	0.09
14 µm	Intercept	0.85	0.45	0.62
	Variable 1	0.84	0.45	0.62
	Variable 2	0.86	0.96	0.90
	Variable 3	0.85	0.93	0.89
	Variable 4	0.84	0.45	0.62
	Variable 5	0.67	0.13	0.54
35 µm	Intercept	1.00	1.00	1.00
	Variable 1	0.90	0.88	0.90
	Variable 2	0.86	0.76	1.00
	Variable 3	0.87	0.72	0.98
	Variable 4	0.92	0.82	0.91
	Variable 5	0.82	0.02	0.49
100 µm	Intercept	1.00	1.00	1.00
	Variable 1	0.00	0.10	0.00
	Variable 2	0.82	0.23	0.00
	Variable 3	NA	0.28	NA
	Variable 4	NA	0.14	NA
	Variable 5	NA	0.01	NA

References

Bogue, R. H., 1922. Contributions to the chemistry and technology of gelatin and glue. Journal of the Franklin Institute, 193(6), 795-825. https://doi.org/https://doi.org/10.1016/S0016-0032(22)90328-X

Fujisawa, N., & Łukomski, M., 2019. Nanoindentation near the edge of a viscoelastic solid with a rough surface. Materials & Design, 184, 108174.

ISO., 2015. Metallic materials — Instrumented indentation test for hardness and materials parameters Part 1: Test method (ISO 14577-1:2015(E)).

Jiang, C., Davis, M., & Zekonyte, J., 2020. Finding Minimal Optimal Indent Separation for Polystyrene via Instrumental Nanoindentation and FEA Method. Applied Sciences, 10(12), 4262. https://www.mdpi.com/2076-3417/10/12/4262

Kremer-Pigmente. 63000-63550 natural sources of glues product data sheet. https://www.kremer-pigmente.com/media/pdf/63000-63550NaturalSourcesOfGlues.pdf

Kremer-Pigmente., 2016. Bone glue (63000) Material Safety Data Sheet. https://www.kremer-pigmente.com/elements/resources/products/files/63000_MSDS.pdf

Kremer-Pigmente., 2020. Bone Glue, pearls 63000 webpage. Mediums, Binders & Glues, 2021(10.05.2021). https://www.kremer-pigmente.com/en/shop/mediums-binders-glues/63000-bone-glue-pearls.html

Oliver, W. C., & Pharr, G. M., 1992. An improved technique for determining hardness and elastic modulus using load and displacement sensing indentation experiments. Journal of Materials Research, 7(6), 1564-1583. https://doi.org/10.1557/JMR.1992.1564

Oliver, W. C., & Pharr, G. M., 2004. Measurement of hardness and elastic modulus by instrumented indentation: Advances in understanding and refinements to methodology. Journal of Materials Research, 19(1), 3-20. https://doi.org/10.1557/jmr.2004.19.1.3

Salvant, J., Barthel, E., & Menu, M., 2011. Nanoindentation and the micromechanics of Van Gogh oil paints. Applied Physics A. Materials Science & Processing, 104(2), 509-515. https://doi.org/10.1007/s00339-011-6486-x

Samuels, L., & Mulhearn, T., 1957. An experimental investigation of the deformed zone associated with indentation hardness impressions. Journal of the Mechanics and Physics of Solids, 5(2), 125-134.

Schellmann, N. C., 2007. Animal glues: a review of their key properties relevant to conservation. Studies in Conservation, 52(sup1), 55-66. https://doi.org/10.1179/sic.2007.52.Supplement-1.55

Sturdy, L. F., Wright, M. S., Yee, A., Casadio, F., Faber, K. T., & Shull, K. R., 2020. Effects of zinc oxide filler on the curing and mechanical response of alkyd coatings [Article]. Polymer, 191, Article 122222. https://doi.org/10.1016/j.polymer.2020.122222

Sudharshan Phani, P., & Oliver, W. C., 2019. A critical assessment of the effect of indentation spacing on the measurement of hardness and modulus using instrumented indentation testing. Materials & Design, 164, 107563. https://doi.org/https://doi.org/10.1016/j.matdes.2018.107563

Tiennot, M., Paardekam, E., Iannuzzi, D., & Hermens, E., 2020. Mapping the mechanical properties of paintings via nanoindentation: a new approach for cultural heritage studies. Scientific reports, 10(1), 7924. https://doi.org/10.1038/s41598-020-64892-7

Wright, M. S., Hudson, M., Kokkori, M., Muir, K., Casadio, F., Faber, K. T., & Shull, K. R. (2014). Quantifying the mechanical properties of artists' paints with nanoindentation. Proceedings of the 2014 Annual Meeting of the Adhesion Society,

Zhao, Y., & Ovaert, T. C., 2010. Error estimation of nanoindentation mechanical properties near a dissimilar interface via finite element analysis and analytical solution methods. Journal of Materials Research, 25(12), 2308-2316. https://doi.org/10.1557/jmr.2010.0295